

Autoclaved aerated concrete reinforced by polymeric pins

✉A. Behenck Aramburu^a, ✉R. de Avila Delucis^b, ✉S. Campos Amico^a

a. Federal University of Rio Grande do Sul, (Porto Alegre, RS, Brazil)

b. Federal University of Pelotas, (Pelotas, RS, Brazil)

✉: arthuraramburu@gmail.com

Received 15 December 2023

Accepted 16 April 2024

Available on line 31 October 2024

ABSTRACT: Autoclaved Aerated Concrete (AAC) is a lightweight and sustainable building material known for its thermal insulation and acoustic properties. However, its relatively low mechanical strength limits its use in load-bearing applications. This paper introduces the concept of incorporating unsaturated polyester resin (UPR) pins into AAC blocks to improve compressive and flexural strength of the material. Pin diameters of 4, 6, 8 and 10 mm were studied, oriented at 90° and 45° in relation to the AAC main plane. The effects of the UPR/AAC interface were analyzed through microscopy. The results point to a substantial increase in mechanical strength of the reinforced AAC, wherein smaller pins with orientation of 45° and 90° presented the best behavior under flexural (up to 298%) and compressive loading (up to 183%), respectively.

KEY WORDS: Autoclaved aerated concrete; Polyester pin; Interface; Lightweight.

Citation/Citar como: Behenck Aramburu A, de Avila Delucis R, Campos Amico S. 2024. Autoclaved aerated concrete reinforced by polymeric pins. Mater. Construcc. 74(355):e350. <https://doi.org/10.3989/mc.2024.370623>

RESUMEN: *Hormigón celular tratado en autoclave reforzado por pasadores poliméricos.* Hormigón celular tratado en autoclave (AAC) es un material de construcción ligero y sostenible conocido por sus propiedades de aislamiento térmico y acústico. Sin embargo, su resistencia mecánica relativamente baja limita su uso en aplicaciones de carga. Este estudio introduce el concepto de incorporar pasadores de resina de poliéster insaturado (UPR) en bloques de AAC para mejorar la resistencia a la compresión y flexión del material. Se estudiaron diámetros de pasadores de 4, 6, 8 y 10 mm, orientados a 90° y 45° en relación al plano principal del AAC. Los efectos de la interfaz UPR/AAC fueron analizados a través de microscopía. Los resultados indican un aumento sustancial en la resistencia mecánica del AAC reforzado, donde los pasadores más pequeños con orientación de 45° (hasta un 298%) y 90° (hasta un 183%) presentaron el mejor comportamiento sobre esfuerzos de flexión y compresión, respectivamente.

PALABRAS CLAVE: Hormigón celular tratado en autoclave; Pasador de poliéster; Interfaz; Peso ligero.

1. INTRODUCTION

Autoclaved Aerated Concrete (AAC) is a construction material composed of cement, fine aggregates (*e.g.*, sand, fly ash, gypsum, and lime), and a foaming agent (*e.g.*, aluminum or zinc powder), which react with calcium hydroxide and water and produce hydrogen gas, creating a lightweight porous structure (1). The AAC is strengthened by autoclaving under steam pressure, in which tobermorite and well-crystallized C-S-H are formed as the main binding phases, improving mechanical strength and durability and reducing shrinkage (2).

AAC blocks have gained increased attention due to their environmentally friendly characteristic compared to conventional building blocks (*e.g.*, fired-clay and conventional concrete blocks), since AAC manufacturing consumes a large volume of important industrial wastes (3). Besides the low density of AAC, with isolated air voids in its porous structure, results in superior sound (4) and thermal (5) insulation, and fire (6), and seismic (7, 8) resistance, making it a good option for various construction applications, including wall systems, flooring and roofing (9). They are also cheap and easy to mold into panels.

AAC has poorer mechanical behavior compared than traditional concrete (10), and its use is limited to applications such as low-rise buildings. Due to that, transverse and longitudinal reinforcements, such as steel bars and meshes, are being incorporated into AAC, to enhance its structural performance. Indeed,

Reinforced Autoclaved Aerated Concrete (RAAC) have wider use in more structural applications. However, steel bars are incompatible with the lightweight characteristic of AAC.

Additionally, the porous structure of AAC exposes the bars to chloride-ion from the environment (*e.g.*, seawater in coastal structures, industrial activities and deicing salts) and highly alkaline conditions, weakening the bond with the concrete and accelerating its deterioration by corrosion (2). In 2023, over 150 schools in the United Kingdom have received instructions to close buildings constructed with AAC reinforced with steel bars until safety measures are implemented. Tens of thousands of these structural panels are currently in use in public buildings, such as hospitals, airports, and theaters, with many showing clear signs of wear and deterioration (11).

In this sense, polymeric materials are interesting candidates as reinforcements for AAC due to their resistance against carbonation (12), good mechanical properties, and low density (13). Unsaturated polyester resin (UPR) is a popular thermoset polymer for composite applications in many sectors (*e.g.*, construction and marine) because of its moderate strength and modulus, resistance to water, and room temperature curing ability (14). UPR has been combined with cement composites in many ways over the last decades. In polymer-impregnated concrete, a typical concrete part is immersed into a liquid polymer solution, that fills the surface voids, reaching polymer penetration depths of 20–50 mm (15–19). Nodehi (19)

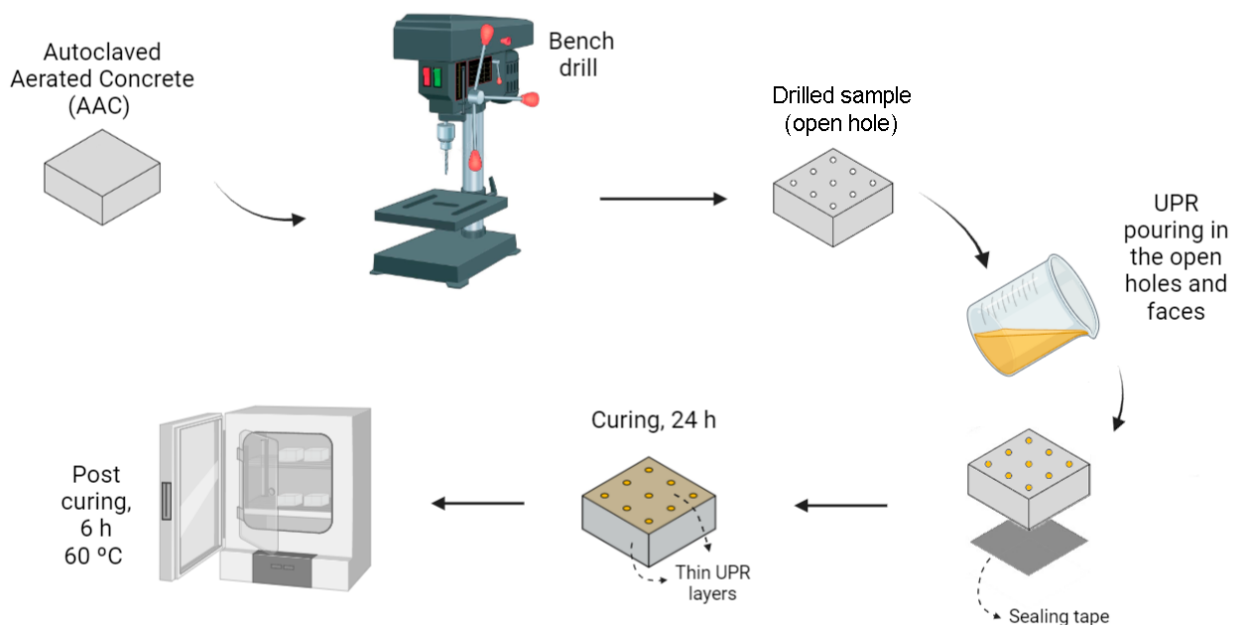


FIGURE 1. Polymeric pin-reinforced RAAC manufacturing.

reported that, depending on the viscosity of the resin, it can enter the micro-pores forming a cross-linked network, which was visualized by Chi *et al.* (20), who studied high-performance epoxy coatings with cross-linkable solvent in concretes.

In fact, the introduction of polymeric pins in composite structures such as sandwich panels, is well-known to improve their load-bearing characteristics, such as flexural (21), compressive (22), and impact (23) behaviors. In this sense, Balikoglu *et al.* (24) investigated the effects of polymeric pins on the performance of a polyvinyl chloride (PVC) foam through three-point bending, flatwise compression, and core shear tests. The pins were found to significantly improve the mechanical performance of the structure, changing failure modes without a significant increase in weight. Similarly, Yalkin, Icten, and Alpyildiz (25) observed the improvement in mechanical performance of a pin-reinforced PVC-core sandwich structure under flexural, shear, compressive, and low-velocity impact loads.

In the context of sandwich panels, the most prevalent pin configurations include those oriented orthogonally (parallel to the load direction) and at $+45^\circ/-45^\circ$ angles, assembling a truss-like structure commonly known as the X-cor (26). Pin reinforcements vary in terms of diameter, spacing, and orientation, resulting in a wide range of design possibilities. According to Zuoguang *et al.* (27), the angle and content of inserted enhance the compressive performance and those oriented at 45° the shear and flexural behavior. Despite the promising results observed for sandwich panels, this possibility remains unexplored for the reinforcement of cement composites, including AAC.

This study aims at using polymeric pin reinforcements to obtain RAAC with different configurations of pins and improved mechanical behavior. This novel approach has the potential of increasing the use of this building material in the construction sector as a lightweight, versatile and mechanically suitable material.

2. MATERIALS AND METHODS

2.1. Materials

Orthophthalic-based unsaturated polyester resin (UPR) with a high content of styrene monomer (41–47%) and low viscosity (140–190 cP) was supplied by Embrapol (Brazil). Methyl-ethyl-ketone peroxide (MEKP) was used as initiator (1.5 wt% in relation to the UPR). Autoclaved aerated concrete (AAC) blocks ($600 \times 300 \times 75$) mm were acquired from Sical (Brazil). According to the manufacturer, the block is produced from a mixture of cement, lime, sand, alu-

minum powder and water. The reaction of aluminum with alkaline components allows the release of hydrogen gas and the expansion of the mixture, forming well distributed small voids. Curing is carried out in autoclaves with controlled temperature and pressure. The AAC density was determined using prismatic specimens based on volume and mass measurements with an analytical scale and analog caliper.

2.2. Pin configurations and manufacturing

For the preparation of reinforced specimens, AAC blocks were cut to predefined dimensions for each mechanical test. Holes were then drilled into the samples using a bench drill, ensuring that they penetrated the entire thickness of the block and that the surface remained free of defects. The specimens underwent vacuum cleaning to ensure surfaces free of debris to facilitate adhesion with the polymer, and an adhesive tape was used to seal the entire bottom surface of the specimens. The UPR and the initiator were mechanically mixed (1000 rpm for 60 s) and manually poured into the holes. Finally, both surfaces were flattened with a thin UPR coating layer, and all specimens were cured at room temperature for 24 h and then post-cured at 60°C for 6 h. The complete process is illustrated in Figure 1.

The holes were drilled to produce pins with diameters of 4, 6, 8, and 10 mm, and the number of pins for each diameter group was determined to ensure a similar resin volume in all specimens, wherein, 36, 16, 9 and 6 pins were used, respectively. Since the number of pins varied in the various samples, the distance between them was defined as to obtain a regular distribution of pins in the specimen for the mechanical tests, *i.e.*, in each sample, the holes were similarly spaced from the borders and from other pins.

Two different configurations of pin orientation were evaluated under both compressive and flexural loading, aiming to optimize the performance under specific conditions. Pins orientations were 90° (aligned to the compressive load) or $-45^\circ/45^\circ$ to form a lattice-like truss structure. In the latter, the horizontal distance between holes was reduced so that the angled pin did not pierce the lateral surface of the block. Finally, unfilled drilled (10 mm diameter) samples for each angle orientation were studied for comparison. Table 1 describes all studied groups of samples.

2.3. Physical characteristics

The pore structure of the AAC blocks was studied by employing image analysis of the inner section of

the block using the ImageJ software. Digital images of the AAC were submitted to thresholding, and the mean pore size and pore area fraction on the AAC were measured. Representative samples of the AAC/UPR interface were analyzed through scanning electron microscopy (SEM) in a Zeiss EVO MA10 equipment at 10 kV using 200–5000× magnification.

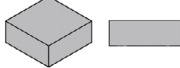
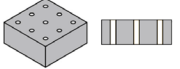
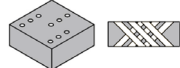
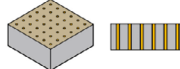
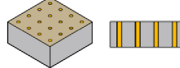
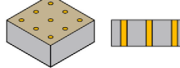
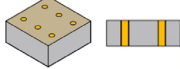
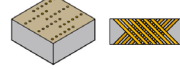
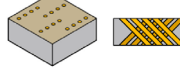
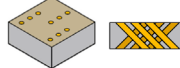
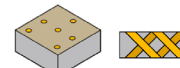
2.4. Mechanical characterization

Tensile tests were carried out in casted samples of the cured polyester resin in accordance with the

ASTM D638 standard (type 1 sample), in an Instron 3382 universal testing machine, at 5 mm/min. Compressive properties were determined in accordance with the ASTM D695 standard, using cylinders measuring 12.30 mm × 24.60 mm (diameter × height) and a displacement speed of 1.3 mm/min. Five specimens were produced, using the same curing conditions mentioned above, and tested in each case.

Mechanical tests were conducted on both as-received (unreinforced) and reinforced AAC using the same Instron universal testing machine. Compression tests followed the recommendations of ASTM C1693 to assess the modulus of rupture and modulus

TABLE 1. Summary of the studied polyester pins reinforced AAC groups

Group	Schematic view and cut	Diameter (mm)	Number	Distance (mm)*	Orientation (°)	UPR/AAC relation (v/v, %)
AAC		-	-	-	-	0
10_90_u		10	9	33.33	90	0
10_45_u		10	9	33.33	45	0
<hr style="border-top: 1px dashed black;"/>						
4_90		4	36	16.00	90	4.52
6_90		6	16	25.00	90	4.52
8_90		8	9	33.33	90	4.52
10_90		10	6	50.00	90	4.71
4_45		4	36	10.00	45	6.38
6_45		6	16	14.00	45	6.38
8_45		8	9	19.33	45	6.38
10_45		10	6	35.70	45	6.65

*Distance between the pin centers.

of elasticity (chord modulus) of the samples (dimensions: $(100 \times 100 \times 35)$ mm) at a displacement rate of 1.5 mm/min. Three-point bending tests were conducted on unreinforced and reinforced AAC to determine the flexural strength in samples (dimensions: $(35 \times 35 \times 160)$ mm), using a span-to-depth ratio of 3, in accordance with ASTM C293. For both mechanical tests, five specimens were used for each group and chord modulus of elasticity was determined between 5% and 33% of the maximum strength for each specimen.

The obtained mechanical properties were statistically analyzed using One-Way ANOVA, in which the characteristics of the pins were considered as a factor. When the null hypothesis was rejected, the means were compared by Tukey-Kramer tests at a 5% significance level based on F and p values. Statistical analysis was performed using Python 3.9 language.

3 RESULTS AND DISCUSSION

3.1. Preliminary characterization

AAC characteristics (*e.g.*, mechanical properties, permeability, and shrinkage) are intrinsically related to overall porosity and pore size distribution (6). Figure 2 presents the untreated and treated micrographs of the as-received AAC, where it can be observed a relatively uniform size and distribution of pores in the AAC. Image analysis indicated 48.2% of pores, ranging from 0.131 to 1.169 mm in diameter, with an average diameter of ≈ 0.519 mm, similar to those reported in the literature (28–30). Also, the measured density was 0.479 g/cm^3 , also similar to literature results (29), being significantly lower than the density of the cured UPR, which is $1.20 (\pm 0.02) \text{ g/cm}^3$.

The mechanical properties of AAC under compressive and flexural loads are shown in Figure 3A, where a substantial contrast is observed with the properties of the UPR (Figure 3B). UPR displayed tensile and compressive strengths of $43.99 (\pm 2.71) \text{ MPa}$ and $124.66 (\pm 5.13) \text{ MPa}$, respectively. Under compressive load, AAC samples exhibited consistent fractures up to the maximum load, where the upper and lower surfaces showed minimal cracks. The failure mode was characterized by shear fractures at $\approx 45^\circ$ near the edges of the prismatic samples, as previously reported in the literature. As the peak stress approaches, shear cracks interconnect, and fine cracks parallel to the loading direction lead to the separation of AAC samples into slender columns (31).

Regarding flexural behavior, it is well-known that cement composites have a much lower tensile strength compared to compressive strength due to crack propagation in flaws inherent to the material. Thereby, when the highly porous AAC underwent tensile stress in the flexural test, the material failed with a brittle behavior with much lower stress than that in compression. Finally, the compressive and the flexural modulus were similar ($\approx 330 \text{ MPa}$).

Due to the characteristics of the UPR used in this research when applied to the AAC surface, its low viscosity enabled it to infiltrate the surface pores effectively. Figure 4 shows the SEM images of the interface between UPR and AAC. Although AAC pores are mostly non-interconnected, some pathways are formed due to interconnected macro and micropores, allowing liquids and gases to flow through it (32). This process is driven by capillary action, forcing the resin to permeate small pores of the AAC (6). Finally, the quality of this type of surface coating and the adhesion between the reinforcing pins and cement matrix depends primarily on a suitable contact and good bonding at the interface.

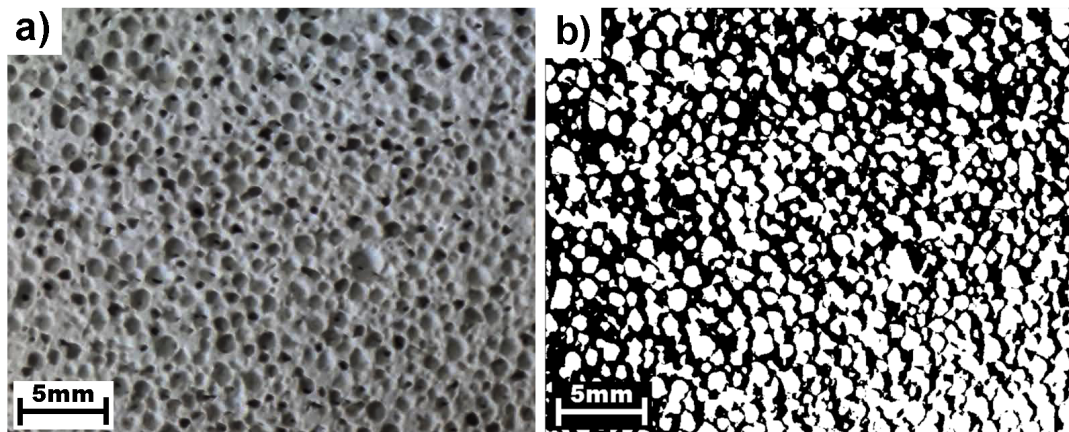


FIGURE 2. Micrograph (a) and thresholding binary image (b) of the as-received AAC.

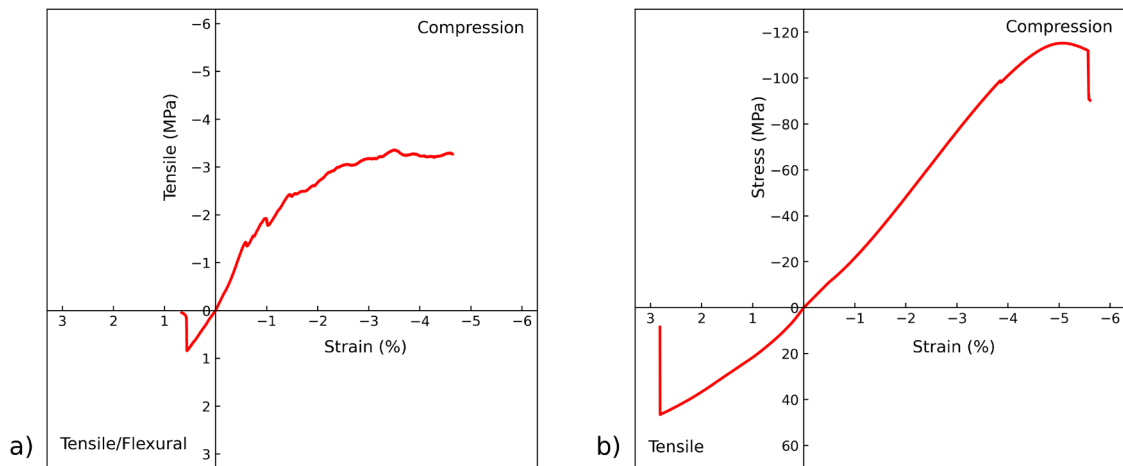


FIGURE 3. Representative stress vs. strain curves for AAC (a) and UPR (b).

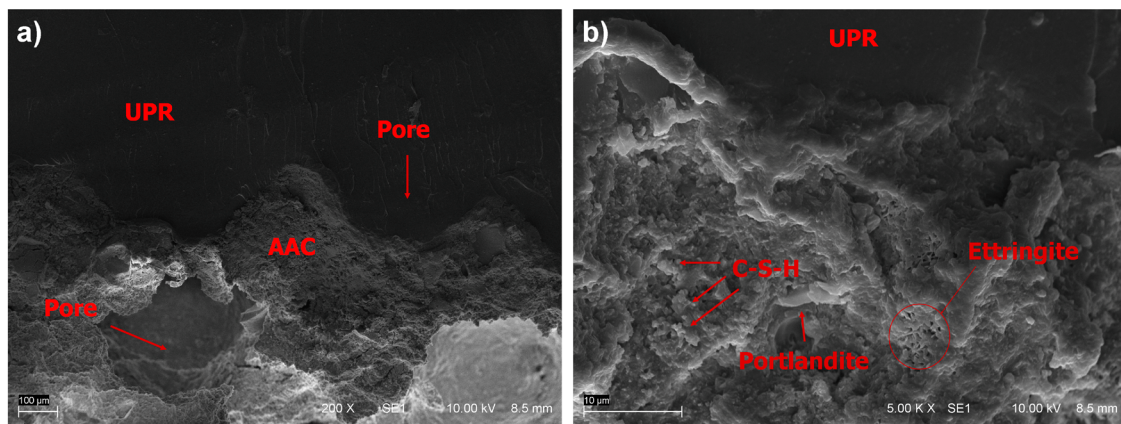


FIGURE 4. SEM images of the interface between UPR and the AAC at (a) 200 \times and (b) 5000 \times magnifications.

Figure 4 shows the pores of AAC, where the resin filled the voids, with little or no trapped air or defects. Thus, good bonding was obtained at the interface, mainly due to mechanical interlocking, where frictional forces between UPR and the rough surface of AAC can promote load transfer. In this sense, the AAC/UPR interface coupled deformation of these two materials. Even so, compatibility between the materials is important, and their modulus of elasticity and thermal expansion coefficients differ significantly.

3.2. Compressive behaviour.

Figure 5 shows the compressive stress vs. strain curves for AACs reinforced with pins oriented at 90°. The unreinforced AAC and the AAC with unfilled holes (10_90_u) exhibited similar behavior, where both compressive modulus and strength were not sta-

tistically different due to the presence of holes. Conversely, the curves for the reinforced groups show a series of small peaks and drops. Although the axial compressive load is uniformly distributed on the surface of the AAC block, the pins may break at different stress levels due to local imperfections. And, when the brittle rupture of a pin occurs, a drop in the curve is observed, leading to stress redistribution to other pins and the AAC, enabling the stress to increase again.

All groups with UPR pins exhibited significantly higher compressive strength and stiffness, with 6.19, 5.24, 4.97, and 4.02 MPa increase in strength for the 4_90, 6_90, 8_90, and 10_90 groups, respectively, compared to the unreinforced AAC (3.38 MPa). The significantly higher compressive strength and stiffness in groups with pin reinforcement can be justified considering the simple rule of mixtures, wherein the properties of the final material are determined by the properties of its individual components and their rel-

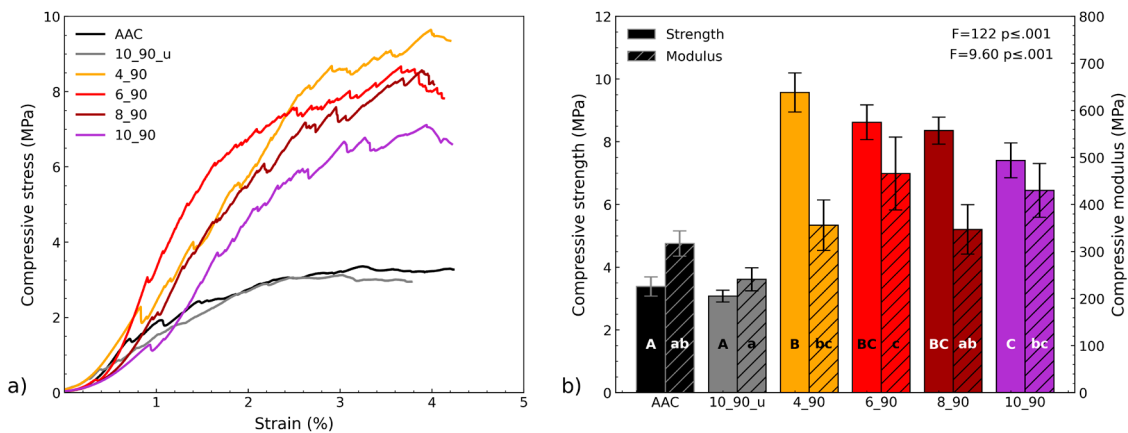


FIGURE 5. (a) Representative compressive stress vs. strain curves and (b) compressive strength and modulus of the blocks with 90° oriented pins (different letters on the bars represent significant differences).

ative content. In this case, the UPR pins exhibit much higher compressive properties than the AAC. With higher stiffness the UPR pins undergo less deformation than the AAC. Consequently, the load is primarily distributed among the pins, contributing to an increase in overall stiffness of the UPR/AAC assembly. Therefore, the enhanced compressive strength and stiffness observed in the pin-reinforced groups can be attributed to the properties of UPR and the effective distribution of load among the pins, as governed by the rule of mixtures.

The failure of pins under compression occurred by brittle rupture and buckling (Figure 6). Buckling was observed only for smaller diameters, *i.e.*, 4 and 6 mm, justified by the slender geometry of the pin. Although buckling is not expected in columns confined by a rigid support, pin buckling occurred after the crack-

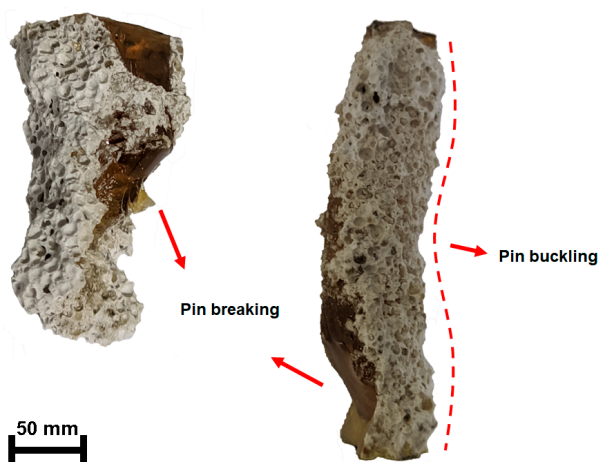


FIGURE 6. Observed 90° oriented pins failure modes due to compressive load.

ing stress of the concrete was reached, wherein the damaged concrete was not able to support the pins. It is important to add that this did not occur for all pins of these groups due to the lateral support of the AAC, preventing buckling (27, 33).

Additionally, there was a trend towards higher compressive strength for smaller pins, based on the statistically significant difference between the 4_90 and 10_90 groups, which may be related to an increased load transfer due to the larger overall surface area of the pins (34, 35). For the larger diameters, brittle fracture was the main failure mode, related to their lower slenderness, emphasizing the influence of geometric factors of the pins on failure mechanisms.

Regardless of the pin diameter, there is an initially uniform load distribution, but after each pin break, stress becomes uneven due to collapsed and non-collapsed regions. Nanayakkara et al. (35) suggested that, in the elastic regime, the pin response under compressive load primarily involves the transfer of interfacial shear stresses. These stresses differ between groups due to the varied pin diameters. For smaller pins, although the sum of areas of all pins is similar to that obtained for the larger pins (see Table 1), their collective surface area in contact with the concrete is much larger, and the total stress transfer is higher, allowing them to share more load prior to AAC break.

The increase in compressive strength for the groups with 45° pins was lower than those oriented at 90° (Figure 7), still reaching 2.35, 1.90, 2.33, and 1.22 MPa increase for the 4_45, 6_45, 8_45, and 10_45 groups, respectively, compared to the unreinforced group. In the group with unfilled holes (10_45_u), unlike that for the unfilled 90° holes, a decrease in elastic modulus was observed. As for compressive strength, all reinforced groups showed statistically similar strengths, but all higher than the unreinforced group.

Unlike the 90° pins, the 45° pins did not break due to the compressive load. As seen in Figure 8, shear cracks near the pins were evident in all reinforced samples, with rupture of the ACC prior to cracking or buckling of the pin, reducing the potential improvement in strength and stiffness. As discussed by Kocher *et al.* (36), pins at 45° exhibit significantly lower stability when subjected to axial compression compared to larger angles (>60°). Therefore, small angles in relation to the surface plane should be avoided for compressive loading, even though they are attractive for flexural loading.

Compared to more conventional reinforcement methods such as the use of fibers, both pins (oriented at 45° and 90°) yielded higher level of reinforcement (37–39). Furthermore, despite the relatively low UPR/AAC ratio in all groups (4.52~6.65%), the pins, the resin permeation into the AAC pores and the flattening layer of material on the faces lead to a mass

increase of approximately 20% and 25% in the groups with pins oriented at 90° and 45°, respectively. Nevertheless, the substantial gain in mechanical strength justifies this increase in mass, maintaining the lightweight characteristic of the original AAC.

3.3. Flexural behaviour

Regarding the flexural strength of the AAC with 90° pins, the groups with larger diameter pins (*i.e.*, 8_90 and 10_90) did not show a statistical difference compared to the unreinforced groups, while the groups with smaller pins (*i.e.*, 4_90 and 6_90) reached gains of 1.82 and 0.92 MPa in strength, respectively (Figure 9).

As observed for compressive loads, geometric irregularities cause higher local stress levels compared to the average stress in the material, potentially

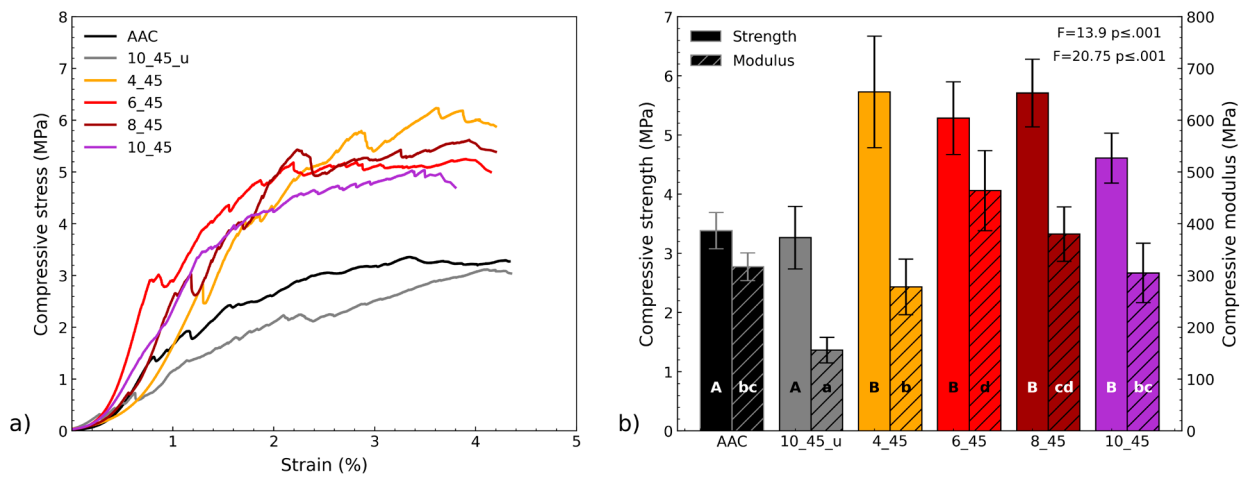


FIGURE 7. (a) Representative compressive stress vs. strain curves and (b) compressive strength and modulus of the 45° oriented pins groups.

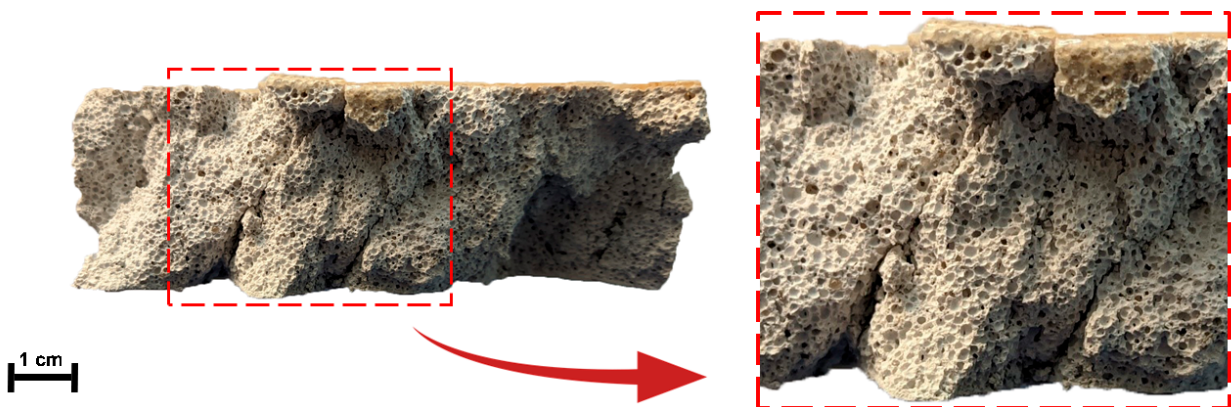


FIGURE 8. Failure mode of the 45° oriented pin groups under compressive load.

leading to cracks or failures. Furthermore, the larger the diameter of the hole, the greater the reduction in load-bearing ability of the structure, potentially altering the failure mechanism (40, 41). Observing the failure modes of the samples with 90° pins (Figure 10), it is evident that the unfilled holes behave as stress concentrators, and rupture occurred in the middle section of the holes (group 10_90_u). Due to that, this group failed at lower deformations than the control AAC group (Figure 9a).

However, in all resin-filled groups, fracture shifted to the regions between pins, in the AAC structure due to the reinforcing effect of the UPR, with higher mechanical properties than the AAC, reinforcing the area near the edges of the pins, displacing the fracture to other areas. This may also be responsible for the increase in modulus in the reinforced blocks, wherein improvements of 234, 233, 128, and 86 MPa were observed for the 4_90, 6_90, 8_90, and 10_90 groups, respectively.

In this sense, under flexural loading, stress concentrations around the pins exceeded the critical stress required for crack initiation, wherein smaller pins, with lower stress concentration effects, allowed higher loads for crack initiation. Moreover, once a crack initiates, smaller pins may hinder crack propagation along the AAC/pin interface. It can also be added that the UPR layer on the surface of the blocks, although very thin, contributed to withstand flexural stress.

Regarding the groups oriented at 45°, shown in Figure 10, since the pins were oriented in two directions (45° and -45°), forming a truss-like geometry, the cracks induced by bending inevitably reached the polyester pins, and these acted as reinforcement until their rupture. This mechanism resulted in increases in strength of 394, 254, and 267 MPa for the 6_45, 8_45,

and 10_45 groups, respectively (Figure 11). In this sense, the diagonal arrangement of pins introduced superior strength and stiffness compared to their respective counterparts oriented at 90°. Indeed, the 90° pins do not effectively counteract shear forces, while the 45° pins reinforce the entire cross-sectional area of the block by changing how shear forces distribute throughout the material, effectively dispersing these forces over a larger area of the material. As for the unreinforced group (10_45_u), since there were no pins to act as reinforcement, the holes behaved again as stress concentrators, causing the blocks to break at lower stress and strain.

It was not possible to obtain the 4_45 group with the manufacturing process employed in this research. These specimens exhibited substantial cracking and deformation due to the polyester significant shrinkage during curing, with a volume contraction that vary from 7% to 10% due to the free radical copolymerization of UPR and styrene, which brings surface quality and dimension control issues. Most shrinkage occur within the first 24 h, when the UPR changes from a viscous liquid to a solid (42). Additionally, being more temperature-sensitive, UPR may exhibit much greater contraction than AAC at low temperatures (43). In fact, the thermal expansion coefficient of UPR is $\approx 10^{-4} \text{ }^\circ\text{C}^{-1}$ (44–46), while that of AAC is only $10^{-5} \text{ }^\circ\text{C}^{-1}$ (47, 48). Due to that, although deformation coupling is beneficial for material reinforcement, it may lead to issues such as interface cracking in this group.

The fact that only this group showed this behavior is likely related to the orientation of the pins and the shape of the flexural specimen. In this regard, inclined pins have a larger volume of resin ($\approx 40\%$ larger than 90° pins) and a closer spacing in the sample.

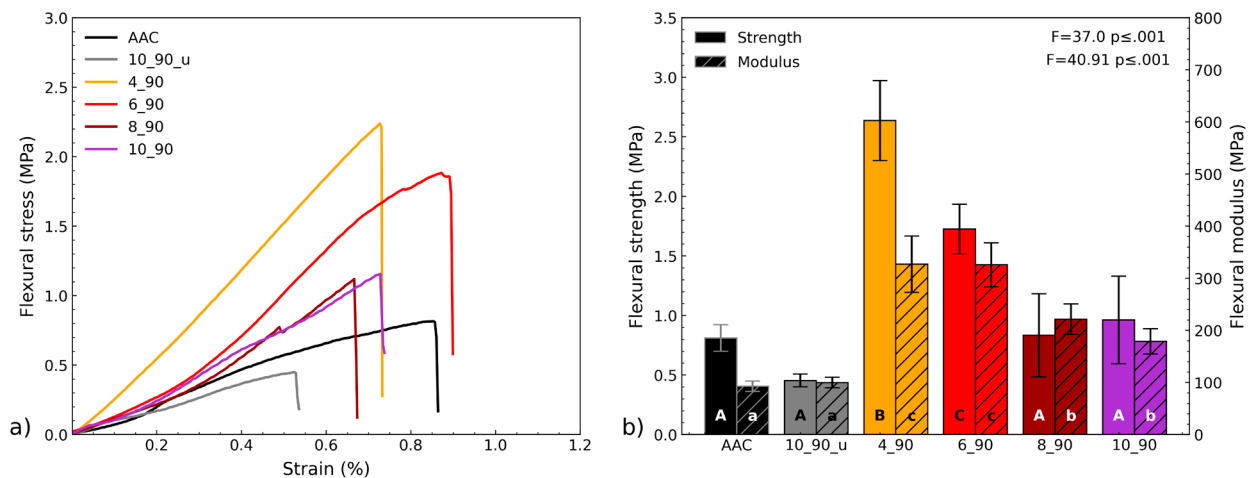


FIGURE 9. (a) Representative flexural stress vs. strain curves and (b) flexural strength and modulus of the 90° oriented pins groups.

The shrinkage of the resin pins causes tensile stresses perpendicular to the interface, and the proximity of the pins led to the rupture of the AAC. In addition, delamination was also observed in the resin layer on the block surfaces due to UPR shrinkage.

Even so, the 6_45 group performed remarkably well. This combination resulted in enhanced flexural properties for both 45° and 90° oriented pins (298% for the 6_45 group and 252% for the 4_90 group), being superior to those found in the literature for fiber reinforced blocks. Indeed, the flexural strength improvement reported by Pehlivanli *et al.* (49) for polypropylene, basalt, carbon, and glass fibers were 40%, 61%, 16%, and 4%, respectively. Similarly, Huang *et al.* (38) incorporated polyethylene fibers and obtained 37% improvement in flexural strength.

Finally, in actual applications, where combined loads may act, it is important to optimize the orientation of polyester pins within AAC blocks to achieve superior overall mechanical behavior. By applying different pin orientations, the material can be engineered to effectively withstand complex loading scenarios with both compressive and flexural loads. For instance, a combination of pins oriented at 45° and 90°, or other angles, could be explored to enhance the structural integrity of AAC blocks against multidirectional forces.

4. CONCLUSIONS

This research focused in improving the compressive and flexural behavior of autoclaved aerated concrete blocks reinforced with unsaturated polyester resin pins. Different sizes of pins oriented at 90° and

45° were evaluated, and the interface between UPR and AAC was assessed. SEM images revealed that the mechanical adhesion between UPR and the AAC matrix resulted in a rough interface that facilitated shear load transfer between them. This interfacial bonding played a crucial role in reinforcing the AAC matrix, resulting in notable improvements in both compressive and flexural strength.

The pins oriented at 90° exhibited the most favorable compression performance, as expected, maximizing load-carrying capacity, with up to 180% improvement. On the other hand, under flexure, the pins oriented at 45° demonstrated superior behavior, achieving up to 298% improvement. Pins at 90° behave better under compression because of their alignment with the applied load direction, while pins oriented at 45° perform better against shear, the most common failure mode under the applied bending conditions.

Furthermore, the choice of pin diameter showed a significant effect on the reinforced AAC. Smaller pin diameters were advantageous in terms of mechanical strength. However, it was observed that the spacing between the pins must be above a minimum to avoid substantial cracks due to resin shrinkage during curing of the polymeric pins.

Acknowledgments

The authors would like to thank the National Council for Scientific and Technological Development – CNPq for the financial support.

Funding Sources

This work was supported by National Council for Scientific and Technological Development (CNPq) (140229/2022-1).

Authorship contribution statement

Arthur Behenck Aramburu: Conceptualization, Data cleansing, Formal analysis, Research, Methodology, Software, Validation, Visualization, Write-up - original draft.

Rafael de Avila Delucis: Conceptualization, Formal analysis, Supervision, Validation, Visualization, Write-up - review & editing.

Sandro Campos Amico: Conceptualization, Formal analysis, Fund raising, Project administration, Resources, Supervision, Validation, Visualization, Write-up - review & editing.

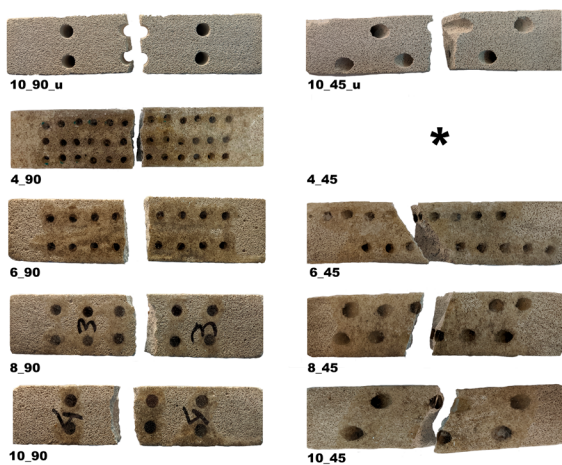


FIGURE 10. Failure modes of 90° and 45° oriented groups observed in the flexural tests. (*broken due to resin shrinkage during curing, not eligible for testing).

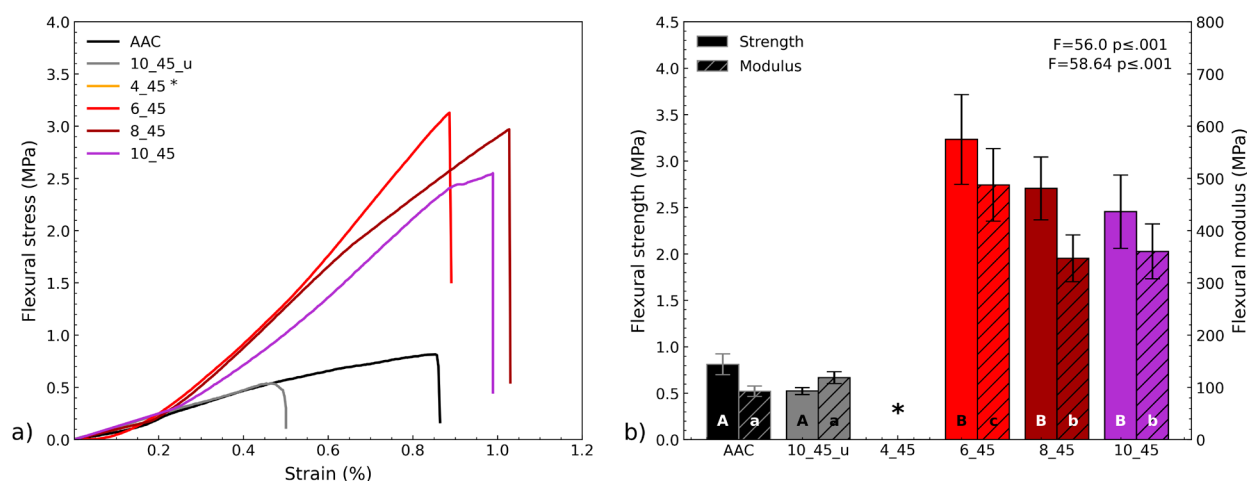


FIGURE 11. (a) Flexural stress vs. strain curves and (b) flexural strength and modulus of the 45° oriented pins groups. (*) broken due to resin shrinkage, not eligible for mechanical testing.

Declaration of competing interest

The authors of this article declare that they have no financial, professional or personal conflicts of interest that could have inappropriately influenced this work.

REFERENCES

- Kalpana M, Mohith S. 2020. Study on autoclaved aerated concrete: Review. *Mater. Today Proc.* 22(3):894–896. <https://doi.org/10.1016/j.matpr.2019.11.099>
- He T, Xu R, Chen C, Yang L, Yang R, Da Y. 2018. Carbonation modeling analysis on carbonation behavior of sand autoclaved aerated concrete. *Constr. Build. Mater.* 189:102–108. <https://doi.org/10.1016/j.conbuildmat.2018.08.199>
- Abhilasha, Kumar R, Lakhani R, Mishra RK, Khan S. 2023. Utilization of solid waste in the production of autoclaved aerated concrete and their effects on its physio-mechanical and microstructural properties: alternative sources characterization and performance insights. *Int. J. Concr. Struct. Mater.* 17(6). <https://doi.org/10.1186/s40069-022-00569-x>
- Yusrianto E, Marsi N, Kassim N, Manaf IA, Shariif HH. 2022. Acoustic properties of autoclaved aerated concrete (AAC) based on Gypsum-Ceramic Waste (GCW). *Int. J. Integr. Eng.* 14(8):67–76. <https://doi.org/10.30880/ijie.2022.14.08.009>
- Emelianov S, Bulgakov A, Otto J, Avakyan A, Protsenko K, Skibin G, Mikheev A. 2023. Fast-hardening slag-alkaline heat-resistant aerated concrete of increased heat resistance with additives of fly ash of novocherkassk SDPP. 149–164. https://doi.org/10.1007/978-3-031-12703-8_16
- Narayanan N, Ramamurthy K. 2000. Structure and properties of aerated concrete: a review. *Cem. Concr. Compos.* 22(5):321–329. [https://doi.org/10.1016/S0958-9465\(00\)00016-0](https://doi.org/10.1016/S0958-9465(00)00016-0)
- Xu C, Nehdi ML, Wang K, Guo Y. 2021. Experimental study on seismic behavior of novel AAC prefabricated panel walls. *J. Build. Eng.* 44:103390. <https://doi.org/10.1016/j.jobe.2021.103390>
- Halici OF, Demir U, Zabbar Y, Ilki A. 2023. Out-of-plane seismic performance of bed-joint reinforced autoclaved aerated concrete (AAC) infill walls damaged under cyclic in-plane displacement reversals. *Eng. Struct.* 286:116077. <https://doi.org/10.1016/j.engstruct.2023.116077>
- Sedaghat A, Soleimani SM, Al-Khiami MI, Sabati M, Rasul M, Narayanan R, Khan MMK. 2023. Development of a novel low-energy building: effects of room orientation and wall materials. *Key Eng. Mater.* 945:101–108. <https://doi.org/10.4028/p-26jy0u>
- Gokmen F, Binici B, Aldemir A, Taghipour A, Canbay E. 2019. Seismic behavior of autoclaved aerated concrete low rise buildings with reinforced wall panels. *Bull. Earthq. Eng.* 17:3933–3957. <https://doi.org/10.1007/s10518-019-00630-3>
- Goodier C, Cavalaro S, Lee K, Casselden R. 2022. Durability variations in reinforced autoclaved aerated concrete (RAAC). Extended Abstract. MATEC Web Conf. 361:06005. <https://doi.org/10.1051/mateconf/202236106005>
- Choi SJ, Bae SH, Lee JI, Bang EJ, Ko HM. 2021. Strength carbonation resistance and chloride-ion penetrability of cement mortars containing catechol-functionalized chitosan polymer. *Materials (Basel)*. 14(21):6395. <https://doi.org/10.3390/ma14216395>
- Patil A, Patel A, Purohit R. 2017. An overview of polymeric materials for automotive applications. *Mater. Today Proc.* 4(2) Part A:3807–3815. <https://doi.org/10.1016/j.matpr.2017.02.278>
- Philips DS, Nair AB. 2023. Unsaturated polyester resins and their classification. In applications of unsaturated polyester resins. Elsevier. 17–24.
- Sarde B, Patil YD. 2019. Recent research status on polymer composite used in concrete-an overview. *Mater. Today Proc.* 18(7):3780–3790. <https://doi.org/10.1016/j.matpr.2019.07.316>
- Ramesh Kumar GB, Rishab Narayanan V. 2020. A review on polymer impregnated concrete using steel wire mesh. *Mater. Today Proc.* 33(1):338–344. <https://doi.org/10.1016/j.matpr.2020.04.118>
- Almusallam AA, Khan FM, Dulaijan SU, Al-Amoudi OSB. 2003. Effectiveness of surface coatings in improving concrete durability. *Cem. Concr. Compos.* 25(4-5):473–481. [https://doi.org/10.1016/S0958-9465\(02\)00087-2](https://doi.org/10.1016/S0958-9465(02)00087-2)
- Liu J, Vipulanandan C. 2001. Evaluating a polymer concrete coating for protecting non-metallic underground facilities from sulfuric acid attack. *tunn. Undergr. Sp. Technol.* 16(4):311–321. [https://doi.org/10.1016/S0886-7798\(01\)00053-0](https://doi.org/10.1016/S0886-7798(01)00053-0)
- Nodehi M. 2022. Epoxy polyester and vinyl ester based polymer concrete: A review. *Innov. Infrastruct. Solut.* 7:64. <https://doi.org/10.1007/s41062-021-00661-3>

20. Chi J, Zhang G, Xie Q, Ma C, Zhang G. 2020. High performance epoxy coating with cross-linkable solvent via diels-alder reaction for anti-corrosion of concrete. *Prog. Org. Coatings*. 139:105473. <https://doi.org/10.1016/j.porgcoat.2019.105473>
21. Zheng Y, Xiao J, Duan M, Li Y. 2014. Experimental study of partially-cured z-pins reinforced foam core composites: K-Cor sandwich structures. *Chinese J. Aeronaut.* 27(1):153–159. <https://doi.org/10.1016/j.cja.2013.07.016>
22. Fojtl L, Manas L, Rusnakova S. 2018. The effect of polymer pin ribs on reinforcement of sandwich structures. *Manuf. Technol.* 18(6):889–894. <https://doi.org/10.21062/ujep/196.2018/a/1213-2489/mt/18/6/889>
23. Kaya G, Selver E. 2019. Impact resistance of z-pin-reinforced sandwich composites. *J. Compos. Mater.* 53(26-27):3681–3699. <https://doi.org/10.1177/0021998319845428>
24. Balıkoğlu F, Demircioğlu TK, Yıldız M, Arslan N, Ataş A. 2020. Mechanical performance of marine sandwich composites subjected to flatwise compression and flexural loading: effect of resin pins. *J. Sandw. Struct. Mater.* 22(6):2030–2048. <https://doi.org/10.1177/1099636218792671>
25. Yalkın HE, İcten BM, Alpyıldız T. 2015. Enhanced mechanical performance of foam core sandwich composites with through the thickness reinforced core. *Compos. Part B Eng.* 79:383–391. <https://doi.org/10.1016/j.compositesb.2015.04.055>
26. Rice MC, Fleischer CA, Zupan M. 2006. Study on the collapse of pin-reinforced foam sandwich panel cores. *Exp. Mech.* 46:197–204. <https://doi.org/10.1007/s11340-006-7103-3>
27. Zuoguang Z, Jijun H, Min L, Yizuo G, Zhijie S. 2009. Mechanical performance of x-truss/foam sandwich construction. *J. Reinf. Plast. Compos.* 28(21):2631–2643. <https://doi.org/10.1177/0731684408093319>
28. Wang Q, Chen Y, Li F, Sun T, Xu B. 2006. Microstructure and properties of silty siliceous crushed stone-lime aerated concrete. *J. Wuhan Univ. Technol. Mater. Sci. Ed.* 21:17–20. <https://doi.org/10.1007/BF02840830>
29. Qu X, Zhao X. 2017. Previous and present investigations on the components microstructure and main properties of autoclaved aerated concrete: a review. *Constr. Build. Mater.* 135:505–516. <https://doi.org/10.1016/j.conbuildmat.2016.12.208>
30. Chen G, Li F, Geng J, Jing P, Si Z. 2021. Identification generation of autoclaved aerated concrete pore structure and simulation of its influence on thermal conductivity. *Constr. Build. Mater.* 294:123572. <https://doi.org/10.1016/j.conbuildmat.2021.123572>
31. Devi NR, Dhir PK, Sarkar P. 2022. Influence of strain rate on the mechanical properties of autoclaved aerated concrete. *J. Build. Eng.* 57:104830. <https://doi.org/10.1016/j.jobe.2022.104830>
32. Laukaitis A, Fiks B. 2006. Acoustical properties of aerated autoclaved concrete. *Appl. Acoust.* 67(3):284–296. <https://doi.org/10.1016/j.apacoust.2005.07.003>
33. Selver E, Kaya G, Dalıf H. 2021. Experimental and theoretical study of sandwich composites with z-pins under quasi-static compression loading. *Adv. Struct. Eng.* 24(12):2720–2734. <https://doi.org/10.1177/13694332211007399>
34. Raeisi S, Kadkhodapour J, Tovar A. 2019. Mechanical properties and energy absorbing capabilities of z-pinned aluminum foam sandwich. *Compos. Struct.* 214:34–46. <https://doi.org/10.1016/j.compstruct.2019.01.095>
35. Nanayakkara AM, Feih S, Mouritz AP. 2013. Improving the fracture resistance of sandwich composite T-Joints by Z-Pinning. *Compos. Struct.* 96:207–215. <https://doi.org/10.1016/j.compstruct.2012.09.029>
36. Kocher C, Watson W, Gomez M, Gonzalez I, Birman V. 2001. Integrity of multi-skin sandwich panels and beams with truss-reinforced cores. 19th AIAA Appl. Aerodyn. Conf. 111–117. <https://doi.org/10.2514/6.2001-1636>
37. Xu R, He T, Da Y, Liu Y, Li J, Chen C. 2019. Utilizing wood fiber produced with wood waste to reinforce autoclaved aerated concrete. *Constr. Build. Mater.* 208:242–249. <https://doi.org/10.1016/j.conbuildmat.2019.03.030>
38. Huang F, Zhang J, Zheng X, Wu Y, Fu T, Easa S, Liu W, Qiu R. 2022. Preparation and performance of autoclaved aerated concrete reinforced by dopamine-modified polyethylene terephthalate waste fibers. *Constr. Build. Mater.* 348:128649. <https://doi.org/10.1016/j.conbuildmat.2022.128649>
39. Onur Pehlivanlı Z, Uzun İ. 2022. Effect of polypropylene fiber length on mechanical and thermal properties of autoclaved aerated concrete. *Constr. Build. Mater.* 322:126506. <https://doi.org/10.1016/j.conbuildmat.2022.126506>
40. Wisnom MR, Hallett SR. 2009. The role of delamination in strength failure mechanism and hole size effect in open hole tensile tests on quasi-isotropic laminates. *Compos. Part A Appl. Sci. Manuf.* 40(4):335–342. <https://doi.org/10.1016/j.compositesa.2008.12.013>
41. Ghasemi AR, Moradi M. 2017. Effect of thermal cycling and open-hole size on mechanical properties of polymer matrix composites. *Polym. Test.* 59:20–28. <https://doi.org/10.1016/j.polymertesting.2017.01.013>
42. Xu L, Lee LJ. 2004. Effect of nanoclay on shrinkage control of low profile Unsaturated Polyester (UP). Resin cured at room temperature. *Polymer (Guildf).* 45(21):7325–7334. <https://doi.org/10.1016/j.polymer.2004.08.051>
43. Gao Y, Zhang H, Huang M, Lai F. 2019. Unsaturated polyester resin concrete : a review. *Constr. Build. Mater.* 228:116709. <https://doi.org/10.1016/j.conbuildmat.2019.116709>
44. Hill RR, Muzumdar SV, Lee LJ. 1995. Analysis of volumetric changes of unsaturated polyester resins during curing. *Polym. Eng. Sci.* 35(10):852–859. <https://doi.org/10.1002/pen.760351007>
45. Aldrighetti C, Tassone P, Ciardelli F, Ruggeri G. 2005. Reduction of the thermal expansion of unsaturated polyesters by chain-end modification. *Polym. Degrad. Stab.* 90(2):346–353. <https://doi.org/10.1016/j.polymdegradstab.2005.01.042>
46. Chieruzzi M, Miliozzi A, Kenny JM. 2013. Effects of the nanoparticles on the thermal expansion and mechanical properties of unsaturated polyester/clay nanocomposites. *Compos. Part A Appl. Sci. Manuf.* 45:44–48. <https://doi.org/10.1016/j.compositesa.2012.09.016>
47. Ullrich A, Garbev K, Bergfeldt B. 2021. In situ x-ray diffraction at high temperatures: formation of Ca2sio4 and Ternesite in recycled autoclaved aerated concrete. *Minerals.* 11(8):789. <https://doi.org/10.3390/min11080789>
48. Jerman M, Keppert M, Výborný J, Černý R. 2013. Hygric thermal and durability properties of autoclaved aerated concrete. *Constr. Build. Mater.* 41:352–359. <https://doi.org/10.1016/j.conbuildmat.2012.12.036>
49. Pehlivanlı ZO, Uzun I, Demir I. 2015. Mechanical and microstructural features of autoclaved aerated concrete reinforced with autoclaved polypropylene carbon basalt and glass fiber. *Constr. Build. Mater.* 96:428–433. <https://doi.org/10.1016/j.conbuildmat.2015.08.104>